MULTILAYER RADIATION SHIELD FOR SATELLITE ELECTRONIC COMPONENTS PROTECTION

Godwin Jacob D' Souza
Associate Professor, Dept. of Electronics, St Joseph's College (Autonomous)
Bangalore.

ABSTRACT

This study presents the development, optimization, and analysis of multi-layer shields tailored for protection against electron and proton space environments. Using the MCNPX code and Genetic Optimization Algorithm, various shield designs are explored, focusing on materials suitable for safeguarding sensitive electronic devices. Through optimization, it's found that the total ionizing dose exceeds that of an aluminum shield by 53.3% for protons and 72% for electrons. Recognizing the significance of proton exposure in Low Earth Orbit (LEO), shield construction prioritizes proton shielding. An exemplary shield is constructed using a combination of Aluminum Bronze and molybdenum layers, supported by a copper carrier. Comparative analysis of radiation attenuation coefficients across experimental, simulation, and analytical results demonstrates strong alignment. These findings underscore the efficacy of the proposed multi-layer shields for safeguarding electronic devices during satellite missions.

KEYWORDS: Optimization Algorithm, various shield designs , Low Earth Orbit (LEO).

INTRODUCTION

Space radiation poses significant challenges in designing space systems, particularly for electronic equipment utilized in satellite missions, as it encounters ionizing particles that can disrupt normal operation. Radiation-induced damage in electronics manifests in three main categories: total ionizing dose (TID), displacement damage (DD), and single event effects (SEE).

To mitigate such risks and ensure mission success, effective countermeasure strategies are essential in space system design. Among these strategies, employing appropriate shielding stands out as a highly effective solution for protecting sensitive electronic components. However, the design of these shields must consider constraints such as satellite mass and volume budgets.

The selection of shielding materials, optimal thickness, layering, and configuration depends on the specific radiation environment encountered. Notably, lightweight materials may not sufficiently attenuate energetic electrons and protons, while heavy materials can produce secondary particles. Therefore, an ideal approach involves combining high-density materials like tantalum and tungsten with low-density ones such as polyethylene.

Monte Carlo methods, including programs like the MCNP code, facilitate the transportation of radiation particles through shielding materials. These computational tools play a crucial role in optimizing shield designs for space systems, ensuring adequate protection against the rigors of space radiation.

The satellite structure serves as the primary radiation shield layer, necessitating careful consideration of factors like weight, vibration tolerance, natural frequency range, and resilience against space radiation during the design phase. In this initial level of protection, the satellite structure absorbs a portion or all of the emitted radiation flux, influenced by its material composition and thickness.

In the subsequent level of shielding, holder boxes, referred to as local shields, are employed. These metal enclosures house electronic boards and sensitive equipment. Due to constraints such as weight and vibration tolerance in satellite structure construction, a significant portion of radiation protection is achieved through the use of holder boxes. Multi-layer shields are implemented to mitigate the secondary effects of impact particles, reflecting the complexity of the space environment, which contains a diverse array of particles. Given the impracticality of replicating such a complex environment in terrestrial laboratories, computational methods serve as effective tools for designing radiation shields.

The significance of this endeavor lies in enhancing the reliability of satellite systems, reducing operational costs, and mitigating project risks. The focus of this research centers on designing radiation shields for use in Low Earth Orbit (LEO) satellites, where trapped electrons and protons constitute the primary sources of space radiation. Consequently, simulation using the MCNPX code incorporates these two particle types, electrons, and protons, under worst-case scenarios.

Figure 1 Schematic of multi-layer radiation shield

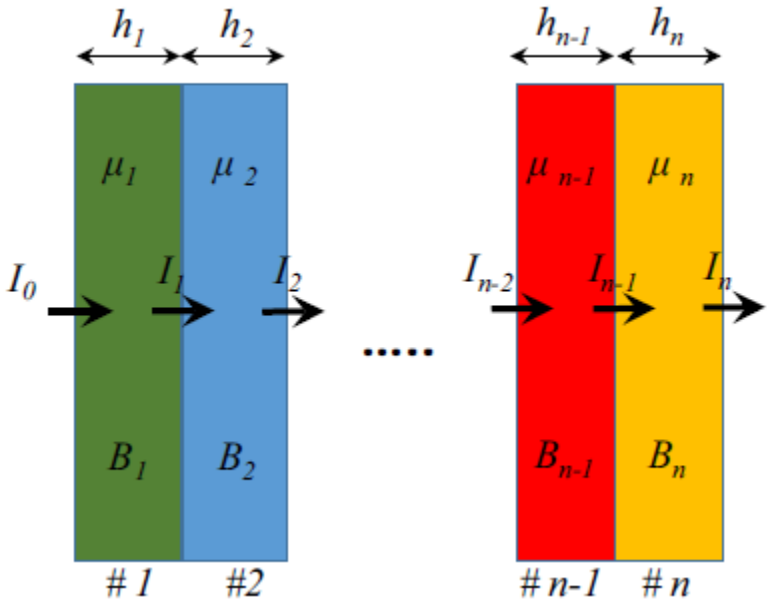

Photons, known for their high penetrating ability, are frequently utilized in experimental setups to simulate worst-case scenarios, with gamma rays being a common choice.

The second and third sections of the paper detail the design of a multi-layer radiation shield structure using Genetic Algorithm (GA) to safeguard electronic devices against electron and proton exposure in space environments, particularly in Low Earth Orbits (LEO). Key parameters include the selection of materials and shield layer thicknesses, crucial for achieving optimal protection against space radiation. In this study, GA generates random numbers for these parameters. The shield structure is then analyzed using the MCNPX code, which provides outputs such as ionization dose, mass, and secondary particles. These outputs are integrated into a cost function in MATLAB for optimization. The optimization process iterates until convergence, refining the thickness and material selection based on

dose and secondary particle considerations. By coupling the MCNPX code with MATLAB, GA optimizes these parameters for electron and proton space environments.

In the fourth section, a three-layer radiation shield is fabricated and tested using commercially available materials, demonstrating practical implementation using off-the-shelf components.

The radiation shields designed for electron and proton space environments demonstrated a shielding effectiveness of 53.3% and 72%, respectively, compared to an aluminum shield of equivalent thickness. Finally, a three-layer radiation shield with a 2 mm thickness was designed and implemented using commercially available off-the-shelf (COTS) materials. The effective protection provided by this structure positions it as a viable candidate for space applications aimed at safeguarding electronic devices.

MULTI-LAYER STRUCTURE DESIGN

In designing shields for space systems, two critical considerations when facing charged particles are minimizing secondary particles resulting from particle collisions with shield materials and reducing the dose received by subsystems. This article investigates how to control these factors based on the nature of the charged particles. Given the greater penetration of photons compared to charged particles, the "attenuation coefficient" becomes a key quantity in shield design, as discussed below.

The schematic of the multi-layer structure is illustrated in Figure 1. When a shield layer is positioned in front of a photon source, such as X- and gamma rays, and considering low absorber thickness and a narrow or well-collimated beam, the gamma-ray flux conforms to the Beer-Lambert equation

$$I = I_0 e^{-\mu} \quad (1)$$

The intensity of the rays after passing through the shield, denoted by I, is related to the initial intensity of the rays, represented by I0, through the Beer-Lambert equation, where x signifies the shield thickness, and μ denotes the radiation attenuation coefficient.

In cases involving wide beams, a correction factor known as the build-up factor, denoted by B, is incorporated into this equation to account for variations.

$$I = BI_0 e^{-\mu} \quad (2)$$

In the scenario of multi-layered shields, the intensity of the radiation source passing through these multiple layers can be described by an equation, as outlined in references 34 and 35.

$$I = B1B2B3I0e-(\mu 1\ x1 + \mu 2\ x2 + \mu 3x3) \quad (3)$$

Multiple analytical and simulation techniques are available to ascertain the radiation attenuation coefficient (μ) of multilayer protections. However, employing transport methods to derive this coefficient is typically limited to straightforward geometries, as demonstrated in several analogous articles across various applications. In this study, the radiation attenuation coefficient is determined using the MCNPX code and the MULASSIS tool, as detailed in references 16 to 20 and 37 to 39.

Table 1 Common materials used for designing the radiation shields.

Number	Material	Density (g/cm3)
1	Tantalum	16.69
2	Tungsten	19.25
3	Lead	11.34
4	Aluminium	2.7
5	Silver	10.49
6	Gold	19.30
7	Copper	8.94
8	Titanium	4.5

Figure 2. Flowchart of the Genetic Algorithm design process

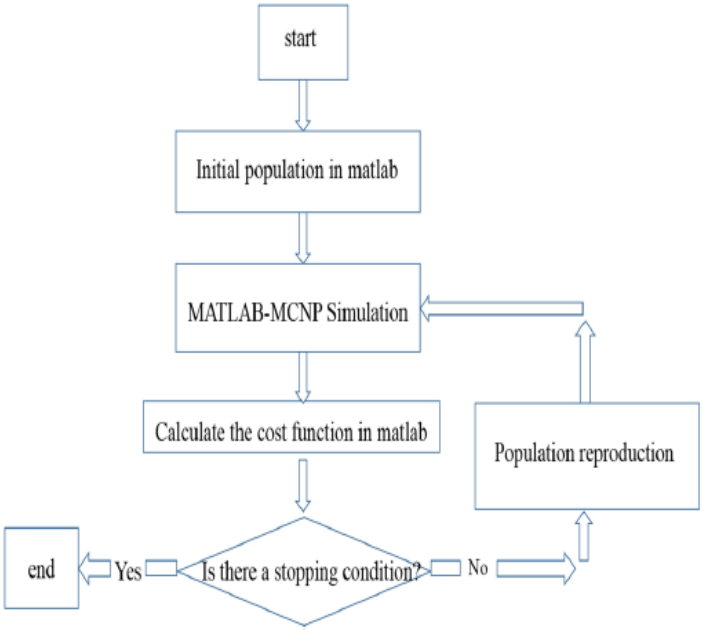

Finally, the XCOM software is employed as an analytical method to determine the attenuation coefficient. By utilizing these three programs - MCNPX code, MULASSIS tool, and XCOM software - it becomes feasible to validate the results effectively.

Table 1 presents a selection of materials commonly reported in literature data for use in radiation shield design. This table includes eight pure materials that are frequently utilized in shield design and are integral to designing and optimizing the proposed multi-layer radiation shielding structures. The cost function for optimization is defined as follows:

$$Cost = \alpha\ X\ TID + \beta\ X\ SP \quad (4)$$

The cost function for optimization is defined by adding the total ionizing dose (TID) and the secondary particles (SP), each multiplied by appropriate weighting coefficients (α and β). TID and SP calculations are conducted using the MCNPX code, where radiation dose is quantified as the energy deposited in the material, expressed in units of energy per mass of material (J/g). To attain an optimal shield, the combination of these two parameters in equation (4) should minimize the cost function. Therefore, an optimization method is necessary. In this case, Genetic Algorithm is employed, requiring a linkage between the MCNPX code and MATLAB software for implementation.

The output of this optimization process includes the thickness of each layer and the corresponding material. The optimization flowchart in Figure 2 illustrates the steps involved in executing this design process.

The combination of the MCNPX code and MATLAB software is utilized to design the optimal shield. Additionally, experimental methods are employed to validate the shield design. Following the design process, the shield is constructed and positioned in front of a radiation source for testing. Flux measurements are taken both before and after shield placement, allowing for the determination of the radiation attenuation coefficient using Equation (1).

In addition to experimental methods, the radiation attenuation coefficient is calculated using computational codes such as MCNPX, MULASIS, and XCOM software. Subsequently, a comparison is made between the radiation attenuation coefficients obtained from experimental and computational methods. If the results closely align, it indicates correct utilization of the MCNPX code. Consequently, the accuracy and validity of the shield design using the combination of MCNPX code and MATLAB are affirmed.

It's worth noting that the simulations consider the electron and proton spectra typical of a common Low Earth Orbit (LEO) satellite. The objective is to design a general, effective multi-layer shield rather than one tailored specifically to a predetermined satellite.

Figure 3. 2D display of the problem structure with a spherical source.

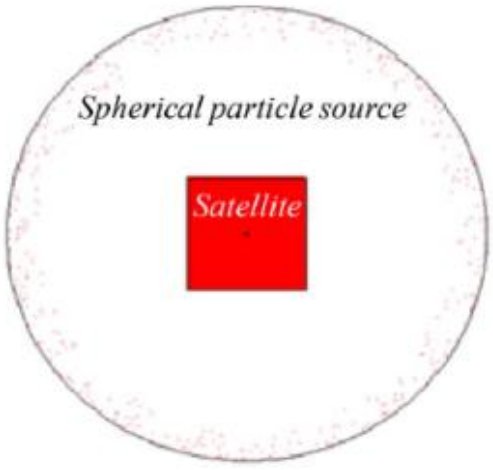

Table 2. Results of Genetic Algorithm for three, five, and seven-layer shields.

Shield types	Specifications	Layers						
		1	2	3	4	5	6	7
Three-layers	Material	Gold	Tungsten	Aluminium				
	Thickness (mm)	1.351	0.339	0.301				
Five-layers	Material	Gold	Gold	Tungsten	Titanium	Titanium		
	Thickness (mm)	0.209	0.856	0.734	0.194	0.012		
Seven-layers	Material	Tungsten	Tantalum	Gold	Tantalum	Tungsten	Titanium	Aluminium
	Thickness (mm)	0.353	0.197	0.481	0.478	0.273	0.182	0.032

Different shields design

In the MCNP simulation process, the satellite platform is modeled as a cube with dimensions of $1 \times 1 \times 1$ m³. The design of an effective shield considers worst-case radiation orbital conditions, with the radiation source conceptualized as a single particle surrounding the satellite spherically. Figure 3 depicts the general structure of the satellite, simulated using the MCNPX code. Notably, the MCNPX code automatically evaluates and achieves the cost function of the Genetic Algorithm (GA) proposed population across generations, facilitated by the linkage between MATLAB and MCNPX.

In the context of a low-dose environment, the focus shifts to the analysis and optimization of radiation shielding for electron environments. Three types of optimizations are undertaken: three, five, and seven-layer shields. These shields are optimized under worst space conditions for electron environments, encompassing electrons within the energy spectrum ranging from 1 to 25 MeV. A single-particle source emitting electrons toward the satellite is considered, resulting in damage to satellite electronics through total ionizing dose and secondary particles.

To minimize the damage induced by these factors, the radiation shield is optimized to minimize the sum of total ionizing dose and secondary particles, as formulated in equation (4). This optimization process accounts for the effects of total ionizing dose, secondary particles, and the number of shield layers. Aluminum is a common material in space hardware, serving both as a radiation shield and structural enclosure. Therefore, the designed multi-layered shields are compared against a 2 mm thickness of aluminum.

The results of these optimizations are summarized in Table 2, showcasing the outcomes for all three optimized shields. Figure 4 illustrates the convergence of the Genetic Algorithm for the three-layer shield, showcasing combinations of high and low-density materials achieved in each case.

Table 3 presents the properties of these three optimized shields from the perspective of total ionizing dose (TID) and secondary particles (SP). The results for TID and SP, displayed in arbitrary units (a.u.), are normalized outputs of Tally in the MCNPX code and are provided solely for comparison purposes. Upon analysis of Table 3, it's observed that the total ionizing dose doesn't exhibit significant differences across all three scenarios. While the seven-layer model shows a slight improvement in dosage, it also entails increased fabrication costs compared to the three-layer configuration. Constructing multi-layer shields with more layers incurs higher costs and introduces technical complexities.

Now that an optimal design has been achieved, it's imperative to evaluate this optimization from various perspectives. The designed shield must effectively mitigate radiation effects across all

energy ranges and outperform an Aluminum shield of equivalent thickness (2 mm) in all electron energy conditions.

In Figure 4, the total ionizing dose passing through both the designed three-layer shield and the Aluminum counterpart is compared for electron sources with varying energies. The plot reveals that the optimized three-layer shield exhibits nearly a 70% improvement in dose reduction compared to the single Aluminum layer. This indicates that the optimized shield not only meets satellite requirements but also holds a significant advantage across all electron energy ranges.

Radiation dose is defined as the energy deposited in the material, with its unit being the ratio of energy to the mass of material, measured in jerk per gram (J/g). Here, 1 jerk equals 1 Giga Joule (GJ).

Figure 4. Curve of total ionizing dose passing through optimal shield and a 2 mm aluminum shield in different energies (the blue curve is related to a three-layer shield)

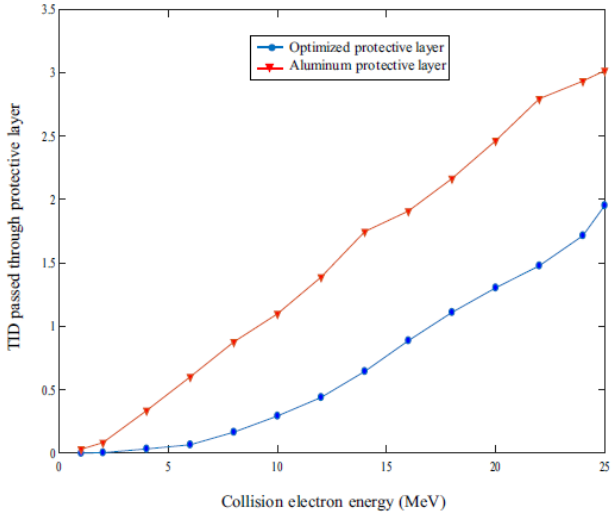

Table 3. Specifications of multi-layer radiation shields and aluminum.

Shield types	Total ionizing dose (a.u.)		Secondary particles (a.u.)	Total thickness (mm)
	Value	Percentage		
Three-layer	$0.5130 \times 10^{-6} \pm 0.03\%$	32	$0.6129 \times 10^{-5} \pm 0.02\%$	1.983
Five-layer	$0.5986 \times 10^{-6} \pm 0.05\%$	38	$0.4071 \times 10^{-5} \pm 0.04\%$	1.985
Seven-layer	$0.4524 \times 10^{-6} \pm 0.06\%$	28	$0.4721 \times 10^{-5} \pm 0.03\%$	1.973
Aluminium	$1.55713 \times 10^{-6} \pm 0.03\%$	100	$0.4013 \times 10^{-5} \pm 0.02\%$	2

Table 4. The results of the GA for three, five, and seven-layer shields.

hield types	Specifications	Layers						
		1	2	3	4	5	6	7
hree-layers	Material	Tungsten	Lead	Tantalum				
	Thickness (mm)	0.705	0.589	0.703				
ive-layers	Material	Gold	Tantalum	Gold	Copper	Copper		
	Thickness (mm)	0.478	0.509	0.211	0.302	0.500		
even-layers	Material	Tantalum	Tungsten	Tantalum	Tantalum	Tungsten	Tungsten	Lead
	Thickness (mm)	0.400	0.352	0.0910	0.393	0.299	0.350	0.108

In this section, the optimization and analysis of radiation shielding for proton environments are discussed, aiming to design shields suitable for worst-case space conditions applicable across various space environments. Proton energies ranging from 1 to 100 MeV are considered in the optimization process. The optimization aims to provide a protective structure optimized in terms of ionization dose, secondary particles, and the number of layers.

The results of Genetic Algorithm optimization for three, five, and seven-layer shields are summarized in Table 4. Additionally, Figure 5 illustrates the convergence of the algorithm for the three-layer shield, showcasing the cost function values versus GA iterations.

Table 5 presents the functional properties of the optimized multi-layer shields and an Aluminum shield for comparison. While the total ionizing dose for the five and seven-layer shields shows only slight improvements compared to the three-layer shield, the total ionizing dose values remain acceptable across all three shields due to the minimal production of secondary particles by protons. Hence, the three-layer shield emerges as a viable, cost-effective option.

Comparing the total ionizing dose in the three-layer shield to that of the Aluminum shield reveals a 50% reduction in dose achieved by the three-layer shielding. Moreover, the three-layer shield outperforms the standard 2 mm Aluminum shield in terms of producing fewer secondary particles.

Figure 5. Convergence curve of GA for three-layer radiation shielding applied for proton space environments.

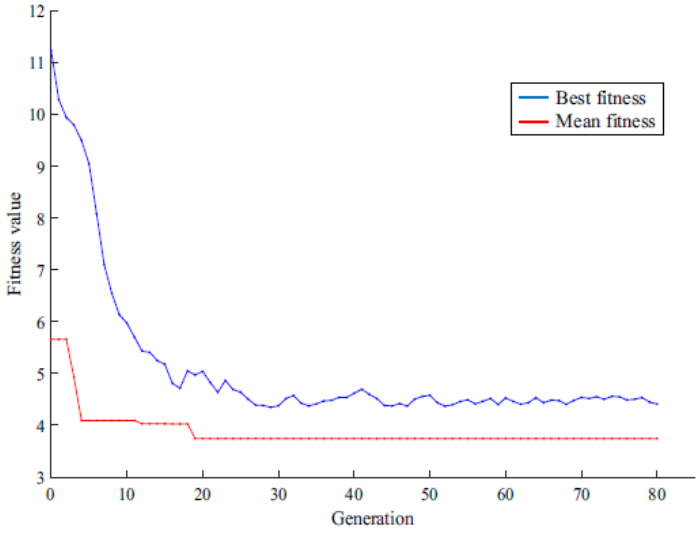

Table 5. Typical specifications of multi-layer radiation and Aluminum shields.

Shield types	Total ionizing dose (a.u.)		Secondary particles (a.u.)	Total thickness (mm)	Fabrication process cost
	Value	Percentage			
Three-layer	2.6926×10^{-6}	50	0.0196×10^{-7}	1.997	Low
Five-layer	2.7066×10^{-6}	50	0.0356×10^{-8}	2	Medium
Seven-layer	2.4867×10^{-6}	46.7	0.0116×10^{-5}	1.993	High
Aluminium	5.3142×10^{-6}	100	0.0458×10^{-5}	2	Low

Figure 6. Total ionizing dose versus particle energy for optimized three-layer and Aluminum shield (the blue curve is related to a three-layer shield)

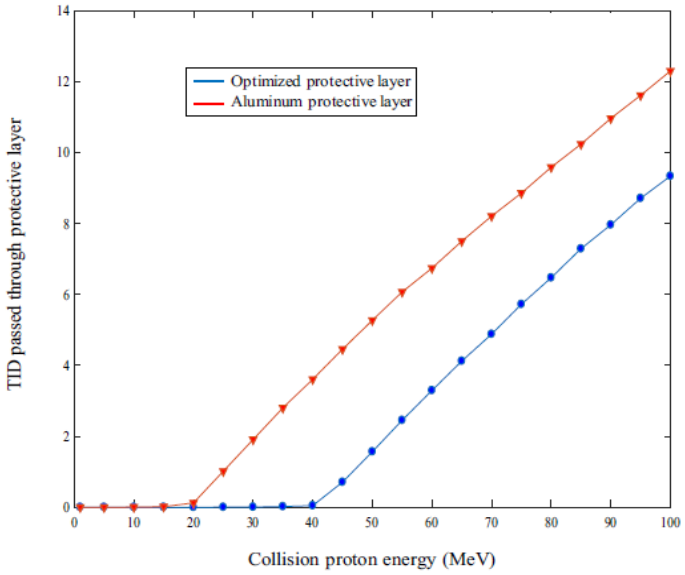

In following figure, the comparison between the total ionizing dose passing through the shielding and Aluminum layers for proton sources across different energy ranges is illustrated. The optimized multi-layer shield demonstrates a 50% improvement over the single Aluminum layer across most cases.

Table 6. The COTS materials used in the optimization process of manufactured radiation shields.

Number	Material	Density
1	Copper	8.94
2	Molybdenum	10.28
3	Aluminium	2.7
4	Tin bronze	8.78
5	Bronze aluminium	8.316

Table 7. specifications of optimized three-layer shield.

Layers	Materials	Thickness (mm)	Density (g/cm3)
Layer-1	Bronze aluminum	0.795	8.316
Layer-2	Molybdenum	0.629	10.28
Layer-3	Bronze aluminum	0.318	8.316

Figure 7. Convergence curve of Genetic Algorithm for constructed shield

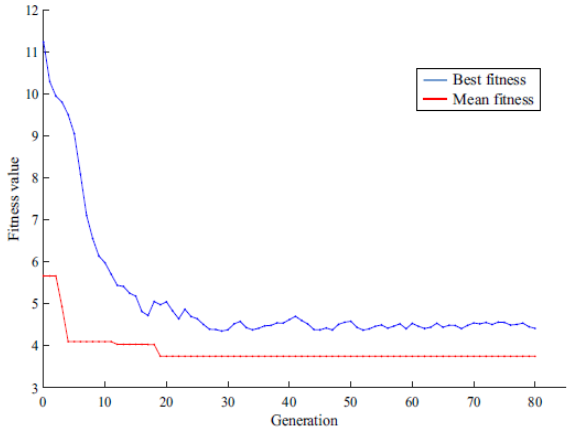

In the transition from design to implementation, practical constraints such as material availability and economic considerations come into play. To demonstrate the real-world application of a three-layer shield, commercially available off-the-shelf (COTS) materials listed in Table 6 are utilized.

For technical feasibility, a copper layer with a thickness of 0.2 mm is selected as the shield carrier. Consequently, the total thickness of the other two layers is adjusted to 1.8 mm. Given the significant impact of proton damage in Low Earth Orbit (LEO) satellites, the study focuses on utilizing proton sources within the energy range of 1–100 MeV.

Optimization results for different layer configurations indicate that the optimal solution is a three-layer shield for interaction with protons. Table 7 presents the specifications of the first, second, and third layers, with the zero layer corresponding to the 0.2 mm copper carrier. The convergence process of the Genetic Algorithm is illustrated in Figure 7.

Fabrication and test

The constructed three-layer shield is realized using the spotting metal method on a 0.2 mm thickness copper sheet, as previously discussed. Figure 8 illustrates the shield sample with dimensions of 5 cm × 5 cm.

Measurements are conducted using a CsI (Tl) scintillator detector model NT-812, as depicted in figure 10. The MCNPX code is utilized to determine the attenuation coefficient through simulation. By comparing the flux in the presence and absence of the radiation shield using Equation (1), the radiation attenuation coefficient is obtained. Additionally, the radiation attenuation coefficient is calculated using the MCNPX code.

In the MCNPX simulation, the detector arrangement (figure 9), radiation shield, and source mimic the experimental setup in the laboratory, as shown in figure 10. This alignment ensures validation of the simulation results for the optimal shield design using the MCNPX code.

During the experimental phase, the CsI (Tl) scintillator detector is employed due to its higher efficiency in detecting gamma rays compared to similar detectors like NaI (Tl), as determined in experimental work. The F2 Tally in MCNPX is used to determine the flux. Additionally, radiation sources with different gamma energies, detailed in Table 8, are utilized for irradiating the proposed shield.

Figure 8. Fabricated three-layer radiation shield sample

Figure 9. Configuration of the source, detector and shield in the MCNPX code.

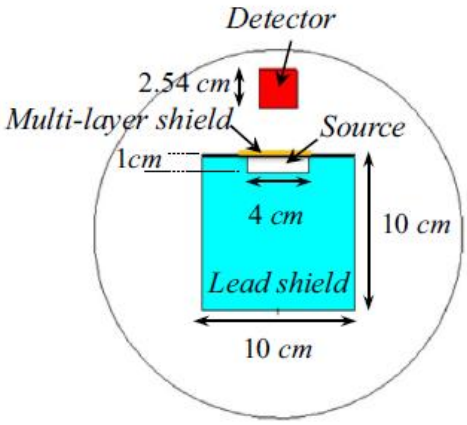

Figure 10. Configuration of irradiation measurement setup using a CsI (Tl) detector (with 1″ × 1″ size of scintillator crystal).

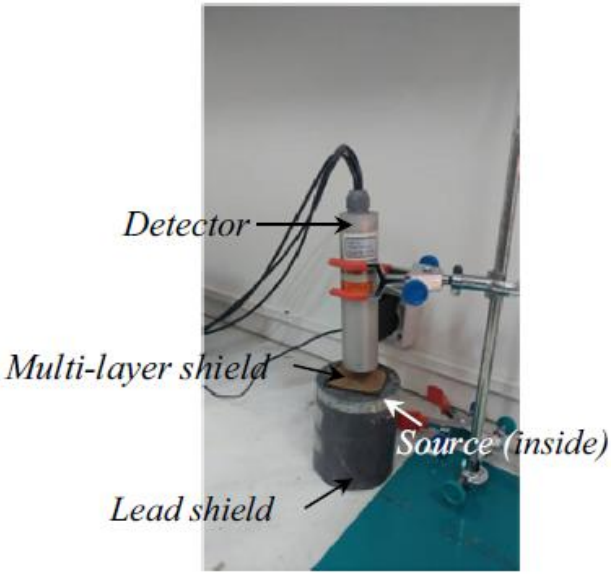

Table 8. Gamma radioisotope sources for irradiation.

Source	Am-241	Ba-133		Co-57	Na-22		Cs-137	Co-60	
Energy (keV)	59	80	356	122	511	1275	662	1173	1333

In figure 10, the setup displays multiple shields positioned between the radiation source and the detector for measurement. The XCOM program aids in calculating the radiation attenuation coefficient across various layers. It incorporates factors such as coherence and non-coherence distribution, photoelectric effects, and pair production. Figure 11 illustrates the mass attenuation coefficient results for Aluminum Bronze, serving as a representative example. Similar results for other materials can be obtained using the same methodology.

Figure 11. Mass attenuation coefficient of Aluminum Bronze using the XCOM.

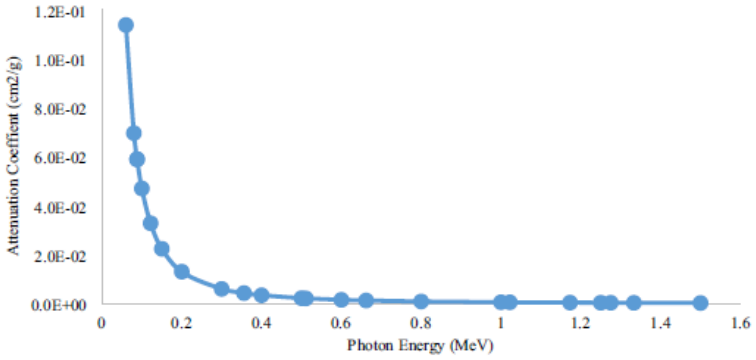

Figure 12. Comparison of attenuation coefficient of Aluminium extracted from XCOM and MCNPX

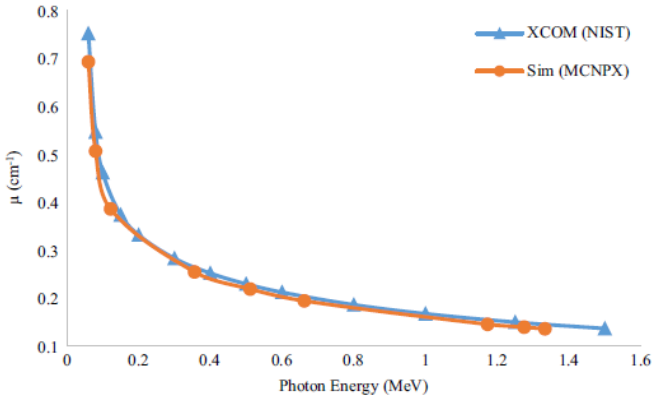

To determine the attenuation coefficient of a multi-layer shield, XCOM is utilized. Assuming B = 1, the radiation attenuation coefficient is calculated through experimental methods and Monte Carlo simulations, employing equation (1). Since XCOM software does not define multi-layered shields, we compare results using the quantity μx, which represents the radiation attenuation coefficient multiplied by the thickness. Thus, this quantity, equivalent to μx in equation (3), is obtained.

$$\mu x = \mu_1 x_1 + \mu_2 x_2 + \mu_3 x_3 + .. \quad (5)$$

To roughly validate the data, we compare the radiation attenuation coefficients derived from both the XCOM program and the MCNPX output. This comparison is conducted for a 2 mm Aluminum shield, utilizing the same geometric setup employed for the multi-layered shield arrangement placed in front of the gamma source, as experimented. The results are depicted in figure 12. Additionally, Table 9 displays the multiplication of the attenuation coefficient of the constituent materials in thickness, or in other words, μx at various energies. These coefficients are obtained using the XCOM online program provided by NIST.

Figure 13 illustrates the results of obtaining the attenuation coefficient of a multi-layer shield through various approaches, including experimental, analytical, and simulation methods. Notably, the output results from the XCOM program and the MCNPX code within the energy range of 0.06–1.5 MeV demonstrate a favorable agreement. Consequently, this comparison extends to a multi-layer radiation shield. The radiation attenuation coefficients obtained from experimental data, XCOM analysis method, Monte Carlo MCNPX code, and MULASSIS tool are depicted in figure 13 for gamma rays.

As depicted in figure 13, the experimental results, XCOM program output, and MCNPX results closely align with each other, whereas values obtained from the MULASSIS tool exhibit noticeable discrepancies. This significant difference can be attributed to the tool's low accuracy in particle transport. MULASSIS, utilized as a module in SPENVIS web-based software, is constrained by the number of transport particles it can handle. Its Monte Carlo and random transport method, coupled with reduced transport particles, increases statistical errors, thus contributing to the disparity with other methods. Another factor contributing to the variance could be the utilization of different cross-sections in libraries. Simulation and statistical methods often assume single-energy sources, while practical sources possess energy spectra. Additionally, factors such as unknown environmental dispersions, detection accuracy, and impurities within the multi-layer shield contribute to computational-experimental disparities. Discrepancies between MCNPX and XCOM results may stem from differences in cross-sections and variations in geometric arrangements, sources, shielding, and detectors.

Table 9. Multiplication of radiation attenuation coefficient of multi-layered shield and thickness using XCOM.

Energy (MeV)	Layer -1 BzAl795	Layer-3 BzAl318	Layer-2 Mo	Layer-0 Cu	μx total
0.06	1.135	0.454	2.764	0.357	4.710
0.08	0.543	0.217	1.269	0.171	2.200
0.1	0.360	0.144	0.709	0.082	1.295
0.122	0.239	0.096	0.434	0.069	0.838
0.15	0.166	0.067	0.272	0.040	0.545
0.2	0.112	0.045	0.157	0.028	0.342
0.3	0.077	0.031	0.089	0.020	0.217
0.356	0.069	0.027	0.075	0.023	0.193
0.4	0.064	0.026	0.068	0.017	0.174
0.5	0.056	0.022	0.057	0.015	0.151
0.511	0.056	0.022	0.056	0.019	0.153
0.6	0.051	0.020	0.051	0.014	0.136
0.662	0.048	0.019	0.048	0.016	0.132
0.8	0.044	0.018	0.043	0.012	0.116
1	0.039	0.016	0.038	0.011	0.103
1.022	0.039	0.015	0.037	0.010	0.102
1.173	0.036	0.014	0.035	0.012	0.097
1.25	0.035	0.014	0.033	0.009	0.092
1.275	0.035	0.014	0.033	0.012	0.093
1.333	0.034	0.014	0.032	0.011	0.091
1.5	0.032	0.013	0.030	0.009	0.084

Figure 13. Comparison of radiation attenuation coefficient of multi-layer shield obtained from experimental, analytical and simulation results

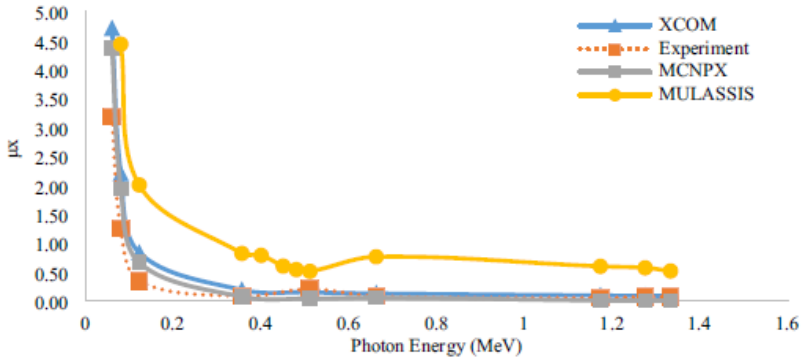

Differences in results can generally be attributed to the presence of multiple layers in the shield's design and construction. These layers introduce complexity to analysis and simulation, rendering the process more challenging compared to single-layer shields. The high consistency observed between experimental and simulation results using the MCNPX code suggests that this trend can be extended to similar cases.

Given that the design and construction of multi-layer shields are based on simulations using this code, and considering the outcomes of nuclear engineering designs conducted with MCNPX, it can be inferred that the simulated built-in shield is suitable for ensuring local shielding and safeguarding electronic components of satellites.

CONCLUSIONS

In this study, various multi-layer shields for space conditions were designed, optimized, and analyzed to protect electronic components against electron and proton environments. The optimization process involved employing the MCNPX Monte Carlo method and Genetic Algorithm to select suitable metals for local shielding. These designed shields were evaluated across different energy levels in space conditions and compared with 2 mm thick Aluminum shields. The results highlighted the superior performance of the optimized shields for electrons, with improvements in total ionizing dose of up to 70%, and for protons, with improvements of up to 50%. Additionally, all designed shields demonstrated potential in reducing the effects of secondary radiations. Optimization efforts were conducted for three, five, and seven-layer shields, with the three-layer shield emerging as advantageous due to its diversity, fewer layers, and lower construction cost. The ultimate optimal configuration was found to be a combination of three layers of Bronze, Aluminum, and Molybdenum. To validate the simulation results, it was necessary to test the shield against proton sources with a maximum energy of 100 MeV. However, due to limitations in using proton sources, gamma radioisotope sources within an energy range of 60–1333 keV were utilized for irradiation. Subsequent validation of experimental results and calculations was conducted using the MCNPX code. The findings revealed a strong correlation between experimental data, simulation, and analytical calculations using both the MCNPX code and the XCOM program. This suggests that the conclusions drawn from this study can be extended to similar cases. Considering that the design and construction of multi-layer radiation shields are based on simulations using the MCNPX code, and given the successful outcomes of nuclear engineering designs conducted with this code, it can be concluded that the simulated built-in shield is suitable for local shielding and ensuring the safety of electronic components in satellites.

REFERENCES:

1. Ashayer, S., Asgari, M. & Afarideh, H. Optimizing gamma-ray shielding material by using genetic algorithm and MCNP code. In 18th International Conference on Nuclear Engineering 325–328 (2010).
2. Alsultanny, Y. A. & Aqel, M. M. Pattern recognition using multilayer neural-genetic algorithm. Neurocomputing 51, 237–247 (2003).
3. Battiston, R. et al. ARSSEM—Active radiation shield for space exploration missions. arXiv:1209.1907 [physics. space-ph] (2012).
4. Berger, M. J. & Hubbell, J. XCOM: Photon Cross Sections on a Personal Computer (National Bureau of Standards, Center for Radia- tion, 1987).
5. Cai, Y., Hu, H., Pan, Z., Hu, G. & Zhang, T. A method to optimize the shield compact and lightweight combining the structure with components together by genetic algorithm and MCNP code. Appl. Radiat. Isot. 139, 169–174 (2018).
6. Chancellor, J. C. et al. Limitations in predicting the space radiation health risk for exploration astronauts. npj Microgravity 4, 1–11 (2018).
7. Gong, J. Zhang, L., Jia, M., Xia, W. & Chen, J. Study on neutron and photon shielding properties of various concretes using MCNP code. In IOP Conference Series: Earth and Environmental Science, 032056 (2018).
8. Kazemi, F. & Malekie, S. A Monte Carlo study on the shielding properties of a novel polyvinyl alcohol (PVA)/WO3 composite, against gamma rays, using the MCNPX code. J. Biomed. Phys. Eng. 9, 465 (2019).
9. Rask, J., Vercoutere, W., Navarro, B. J. & Krause, A. Space Faring: The Radiation Challenge, An Interdisciplinary Guide on Radiation and Human Space Flight (NASA Marshall Space Flight Center, 2008).
10. Stephens, D. Jr., Townsend, L., Miller, J., Zeitlin, C. & Heilbronn, L. Monte Carlo transport model comparison with 1A GeV accel- erated iron experiment: heavy-ion shielding evaluation of NASA space flight-crew foodstuff. Adv. Space Res. 30, 901–905 (2002).
11. Taylor, B. et al. The micro radiation environment monitor (MuREM) and SSTL radiation monitor (SSTL RM) on TechDemoSat-1. IEEE Trans. Nucl. Sci. 59, 1060–1065 (2012).
12. Sharma, M. K., Alajo, A. B. & Liu, X. MCNP modeling of a neutron generator and its shielding at Missouri University of Science and Technology. Nucl. Instrum. Methods Phys. Res. Sect. A 767, 126–134 (2014).